Editors' Suggestion

Topological Order in an Antiferromagnetic Tetratic Phase

Daniel Abutbul and Daniel Podolsky
Physics Department, Technion, 32000 Haifa, Israel

(Received 19 December 2021; revised 11 April 2022; accepted 2 June 2022; published 23 June 2022)

We study lattice melting in two-dimensional systems of spinful particles that interact antiferromagnetically. We argue that, for strong spin interactions, single lattice dislocations are forbidden by magnetic frustration. This leads to a melting scenario in which a tetratic phase, containing free dislocation *pairs* and bound disclinations, separates the solid from the liquid. We demonstrate this phase numerically in a system of hard spheres confined between parallel plates, where spins are represented by the heights of the spheres. In the tetratic phase, the spins are shown to be as antiferromagnetically ordered as allowed by their spatial configuration.

DOI: 10.1103/PhysRevLett.128.255501

In typical solid-state antiferromagnets (AF), the Néel temperature is significantly lower than the melting temperature of the crystal. For this reason, spin interactions do not play a role in the crystal melting. But what would happen if the AF interactions were to be comparable, or even dominant, over the interactions responsible for the crystal ordering? Would this change the nature of the melting transition? One naively expects melting to be a direct transition from an AF solid to a magnetically disordered liquid, as it is difficult to envision lattice melting that does not destroy antiferromagnetism.

In this Letter, we demonstrate that another possibility exists in two dimensions (2D): the solid and liquid phases could be separated by an intermediate phase, a topologically ordered tetratic. This phase has strong AF correlations that survive the partial melting of the lattice. We will first give a general argument for this phase, based on a modification of the Kosterlitz-Thouless-Halperin-Nelson-Young (KTHNY) picture of defect-mediated melting [1–3]. This will be complemented by a numerical demonstration of this phase in an experimentally realizable microscopic system, a collection of hard spheres confined between parallel plates.

The proposed tetratic phase is unusual. In it, single dislocations bind into free dislocation *pairs*, such that double dislocations (of Burgers vector $|\mathbf{b}| = \sqrt{2}$) are free, while fundamental ($|\mathbf{b}| = 1$) dislocations remain bound. In this sense, the tetratic is topologically ordered, since higher-charge topological defects proliferate while the fundamental defects do not [4–8].

Tetratic phases have been previously observed [9–19], including in a closely related system of Hertzian spheres [20]. However, the possibility of topological order, if present, has not been explored. Evidence for binding of defects was seen in bilayer systems of interacting particles [21], although the tetratic phase was not observed. Previous works considered the possibility of topological order [22] and AF order [22,23] in molten phases, but did not demonstrate these behaviors microscopically.

We begin by considering the effect of strong AF interactions on the topological defects of a crystal.

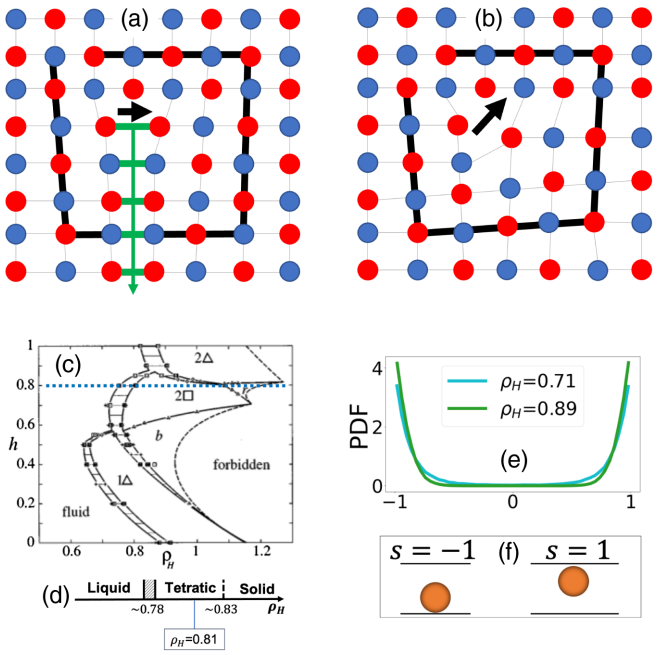

FIG. 1. (a) A single dislocation in AF lattice creates a string of unsatisfied bonds (green). Burgers circuit shown by a thick black line. (b) At a double dislocation, no string is created. (c) Phase diagram of confined hard spheres (adapted from Ref. [27]). (d) Phase diagram at $h = 0.8$, as obtained in current work. We focus on an intermediate density $\rho_H = 0.81$, shown to be a topologically ordered tetratic. (e) Probability density function of the normalized sphere heights, at two extreme values of ρ_H. The spheres are seen to stay close to the confining plates. (f) Spin representation of the spheres: the upper or lower layer is associated with $s = \pm 1$.

Consider a system of particles with Ising spins whose ground state is a Néel state on the square lattice. As shown in Fig. 1(a), a fundamental dislocation breaks the bipartiteness of the lattice and introduces frustration by forcing a semi-infinite string of unsatisfied bonds (across which spins are aligned) to emanate from the dislocation core [24–26]. This costs energy that grows linearly with system size, overwhelming the logarithmic free-energy gain associated with the entropy of the dislocation. Hence, the AF background prohibits fundamental dislocations from occurring in isolation. By contrast, a *double* dislocation [Fig. 1(b)] has a Burgers vector $|\mathbf{b}| = \sqrt{2}$ that connects two spins of the same sublattice. Therefore, it preserves bipartiteness and does not cause frustration [24]. Hence, although double dislocations cost more lattice energy than fundamental dislocations, they do not cost magnetic energy, and they can therefore proliferate when the entropic gain is large enough. Within the KTHNY scenario, a topologically ordered tetratic then results, provided the disclinations remain bound.

Having described the mechanism underlying the topologically ordered tetratic, we turn to the question: Does this phase occur in an experimentally realizable microscopic model? To obtain strong AF interactions, we look for a system in which the AF and crystallization interactions have a common origin. One such candidate is a collection of hard spheres confined between parallel plates. The spheres do not have internal degrees of freedom. However, when the separation between plates H is larger than the sphere diameter σ but smaller than 2σ, one can think of the height of the spheres relative to the center plane as an effective "spin." In what follows, we will use the terms "solid," "liquid," and "tetratic" to refer to the 2D configuration of the spheres in the plane, without regard to their out-of-plane heights; these will be referred to as their spin. The spheres are noninteracting, other than a hard-core repulsion which forbids overlaps. However, thermally induced entropic forces favor configurations in which the spheres pack well. This gives rise to effective AF interactions between spins, since two nearby spheres can get closer to each other when their heights are different. This system has been studied as a model of AF Ising spins on a hexagonal lattice and can be realized experimentally using colloids [28,29].

Since height is a continuous variable, the effective spins are soft. However, the spheres in practice lie close to the confining plates [Fig. 1(e)], making the hard spin assignment $s = \pm 1$ a good approximation [Fig. 1(f)].

The phase diagram for this system [Fig. 1(c)] was computed in Ref. [27] (the possibility of intermediate phases—tetratic or hexatic—was not considered). The phase diagram is characterized by two dimensionless parameters: the normalized density ρ_H and plate separation h, defined by $\rho_H = (N\sigma^3/AH)$ and $h = (H/\sigma) - 1$. Here, N is the number of spheres and A is the total area. For $h = 0$ the system is strictly 2D, and the spheres arrange in a hexagonal solid. As the plate separation is increased, $h > 0$, the out-of-plane fluctuations increase, and so do the effective AF interactions. These can become strong enough to modify the 2D lattice into a bipartite lattice, in order to resolve the magnetic frustration of the hexagonal lattice. This is an indication that the magnetic and lattice elastic energy scales are comparable in this system. In our work, we focus on $h = 0.8$, where the preferred solid over a wide range of densities is a square lattice (at large values of ρ_H, a rhombic structure is preferred due to further-neighbor interactions).

To thermalize the spheres, we use the event-chain Monte Carlo algorithm [30], as it equilibrates quickly and succeeds in escaping local minima [31,32]. We extend the 2D straight event-chain algorithm, described in Ref. [30], to three dimensions. In our extension, we apply cyclic boundary conditions along $\hat{x}$ and $\hat{y}$ and hard-wall conditions in the $\hat{z}$ direction: When a sphere hits a wall, it bounces back (see the Supplemental Material [33]).

At $h = 0.8$, as the sphere density is reduced starting from $\rho_H = 0.9$, we find a sequence of transitions from square lattice solid, to tetratic, to liquid. We locate the critical densities at the transitions by looking for a change of the correlation functions, from algebraic to exponential decay. At the solid to tetratic, the change is in the positional correlations, $g_k(r)$; at the tetratic to liquid, the change is in the bond-orientational correlations $g_4(r)$ [20,34,35]. These correlation functions are obtained from corresponding complex-valued order parameters, as described next.

The positional order parameter, evaluated at the location of sphere α, is defined with respect to a vector $\bar{\mathbf{k}}$ in the reciprocal lattice by $\psi_{\bar{\mathbf{k}}}(\alpha) = e^{i\bar{\mathbf{k}}\cdot\mathbf{r}_\alpha}$ [2], where $\mathbf{r}_\alpha = (x_\alpha, y_\alpha)$ is the lateral position of the sphere's center, ignoring its height. The value of $\bar{\mathbf{k}}$ may deviate slightly from that of a perfect lattice of the given density, due to lattice defects [31]. Instead, we choose $\bar{\mathbf{k}}$ at the numerically evaluated Bragg peak, which maximizes the static structure factor $S(\mathbf{k}) = (1/N)|\sum_\alpha \psi_{\mathbf{k}}(\alpha)|^2$. The bond-orientation order parameter of the square lattice is defined by $\psi_4(\alpha) = \frac{1}{4}\sum_{\beta\in \mathrm{NN}(\alpha)} e^{4i\times\theta_{\alpha\beta}}$ [27], where $\beta \in \mathrm{NN}(\alpha)$ runs over the four nearest neighbors of the sphere α, and $\theta_{\alpha\beta}$ is the angle between the bond vector $\mathbf{r}_\alpha - \mathbf{r}_\beta$ and the $\hat{x}$ axis. The correlation $g(r)$ of a complex field $\psi(\mathbf{r})$ is defined as the product of the field at points a distance r from each other: $g(r) = \int (d^2\mathbf{r}_\alpha d^2\mathbf{r}_\beta/A)\{[\delta(|\mathbf{r}_\alpha - \mathbf{r}_\beta| - r)]/2\pi r\}\psi^*(\mathbf{r}_\alpha)\psi(\mathbf{r}_\beta)$. As, in practice, we have only samples of the continuous field $\psi(\mathbf{r})$ at discrete positions $\mathbf{r}_\alpha$, we use binning of $\psi^*(\alpha)\psi(\beta)$ according to the histogram of separations between pairs of spheres $|\mathbf{r}_\alpha - \mathbf{r}_\beta|$. The correlation of $\psi = \psi_4$ is denoted by $g_4(r)$ and that of $\psi = \psi_{\bar{\mathbf{k}}}$ by $g_k(r)$.

Figure 2 shows correlations for various values of ρ_H. The change in $g_k(r)$ from algebraic to exponential decay happens at $\rho_H \approx 0.83$. The onset of exponential decay in $g_4(r)$ happens at $\rho_H \approx 0.78$. This leaves an intermediate

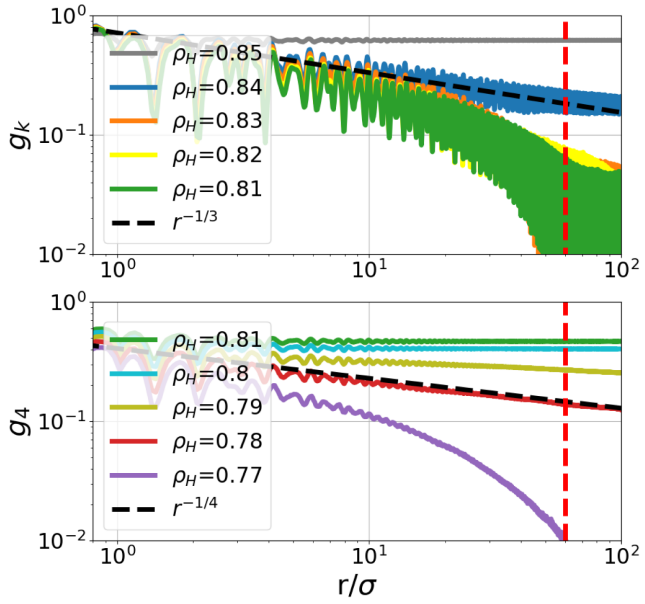

FIG. 2. Positional (g_k) and orientational (g_4) correlations for constant plate separation $h = 0.8$ and varying density ρ_H, for a system with $N = 90,000$ spheres (the system size at $\rho_H = 0.8$ is $250\sigma \times 250\sigma \times 1.8\sigma$). Exponential decay of correlation is observed at $\rho_H \leq 0.83$ for the positional correlation (upper panel) and $\rho_H \lesssim 0.78$ for the bond-orientational correlation (lower panel). The $r^{-1/3}, r^{-1/4}$ bounds from the hexagonal lattice are shown for reference. The features beyond the dashed red line are associated with finite size effects.

tetratic phase for $0.78 \lesssim \rho_H \leq 0.83$. We note here that the tetratic should show algebraic decay in $g_4(r)$, whereas we seemingly obtain nondecaying correlations at $\rho_H = 0.81$ [as we do in $g_k(r)$ at $\rho_H = 0.85$, which lies in the solid phase]. Similar results were obtained for the hexatic in Refs. [31,35], and may be attributed to very slow algebraic decay. For the hexagonal lattice, bounds exist for the decay rate of $g_k(r)$ in the solid ($r^{-1/3}$), and of $g_4(r)$ in the hexatic ($r^{-1/4}$) [2,34]. For the square lattice, however, we do not know of such rigorous bounds [20]. Also note that topological order is expected to change these power laws. In Fig. 2, we display the standard power laws for the hexagonal lattice as a guide to the eye, only.

We next consider the transition from the tetratic to the liquid, which occurs near $\rho_H \approx 0.78$. At $\rho_H = 0.78$, the orientational correlations look algebraic. However, at this density, we cannot rule out phase coexistence: we observe bimodal histograms of the orientational order parameter ψ_4, as well as proliferation of grain boundaries (see the Supplemental Material [33]). This suggests that the tetratic to liquid transition is first order [35] (finding a Mayer-Wood loop in the equation of state would settle this more definitely [14]). A similar scenario, of a continuous solid to *hexatic* transition, followed by a first order hexatic to liquid transition, was observed in hard disks in 2D [31,32,35], and in 2D regular polygons [9].

Having found a tetratic phase, we move on to demonstrate that it is topologically ordered, in the sense of only containing free $|\mathbf{b}| = \sqrt{2}$ dislocations. To visualize the dislocation field $\mathbf{b}(\mathbf{r})$ in the system, we implement a 2D dislocation extraction analysis code (DXA) following Ref. [36]. We first rotate our system by the angle $-\frac{1}{4}\arg\left((1/N)\sum_\alpha \psi_4(\alpha)\right)$, thus aligning the average bond orientation with the $\hat{x}$ axis. We then perform a Delaunay triangulation of the sphere lateral positions. Then, for each triangle $\alpha\beta\gamma$ of the triangulation, we compute whether it contains a dislocation. For this, we define the set of separation vectors between nodes of the perfect square lattice, $S' = \{(na, ma)|(n, m) \in \mathbb{Z}^2\}$, where $a = (2\pi/|\bar{\mathbf{k}}|)$ is the lattice constant. Then, for each edge vector of the triangle, $\mathbf{\Delta}_{\alpha\beta} = \mathbf{r}_\alpha - \mathbf{r}_\beta$, we find the nearest vector $\mathbf{\Delta}'_{\alpha\beta} \in S'$ within this set. Finally, the Burgers vector is given by $\mathbf{b}_{\alpha\beta\gamma} = \mathbf{\Delta}'_{\alpha\beta} + \mathbf{\Delta}'_{\beta\gamma} + \mathbf{\Delta}'_{\gamma\alpha}$.

In the tetratic phase, at $\rho_H = 0.81$, we indeed find that the free dislocations all have Burgers vector $|\mathbf{b}| = \sqrt{2}$, as shown in Fig. 3(a). To be more precise, the overwhelming majority of dislocations obtained from DXA have a unit Burgers vector. However, these tend to appear as bound dislocation-antidislocation pairs, or as larger local clusters whose total Burgers vector sums to zero, as illustrated in Fig. 3(b). To clean those neutral groups, we first remove neighboring dislocation-antidislocation pairs recursively. We then use a single-linkage agglomerative clustering algorithm [37] (see the Supplemental Material [33] for more details). At the end of this procedure, we find clusters that are either neutral, or have a total $\sqrt{2}$ Burgers vector, indicating topological order. The free double dislocations are shown in Fig. 3(a), with colors according to their orientation. As a check that the cleaning procedure does not bias toward double dislocations, we run the same analysis on mock data consisting of randomly scattered single dislocations and bound pairs. We find that, by contrast to the tetratic, in this case nearly all of the final clusters have a unit Burgers vector.

Having demonstrated topological order, we next study the antiferromagnetism in the tetratic phase. As argued above, double dislocations preserve bipartiteness. Therefore, it may be possible, in principle, for the tetratic phase to have true long-range AF order [22–24]. It is difficult to give a precise definition of long-range AF order in the tetratic phase. The usual definition involves the spin-spin correlation function $s_i s_j e^{i\mathbf{K}\cdot(\mathbf{r}_i - \mathbf{r}_j)}$, where $\mathbf{K} = (\pi/a, \pi/a)$ for a square lattice. However, in the tetratic phase, $e^{i\mathbf{K}\cdot(\mathbf{r}_i - \mathbf{r}_j)}$ decays exponentially. This makes the spin-spin correlation function, as defined above, short ranged *regardless* of the spin configuration. Nonetheless, in practice we find fairly sharp peaks in the magnetic structure factor, $S^M(\mathbf{k}) = (1/N)\sum_{i,j} s_i s_j e^{i\mathbf{k}\cdot(\mathbf{r}_i - \mathbf{r}_j)}$, as shown in Fig. 4. As the thermodynamic limit is approached, these peaks are expected to eventually spread out into a ring due to the lack of orientational long-range order. Interestingly,

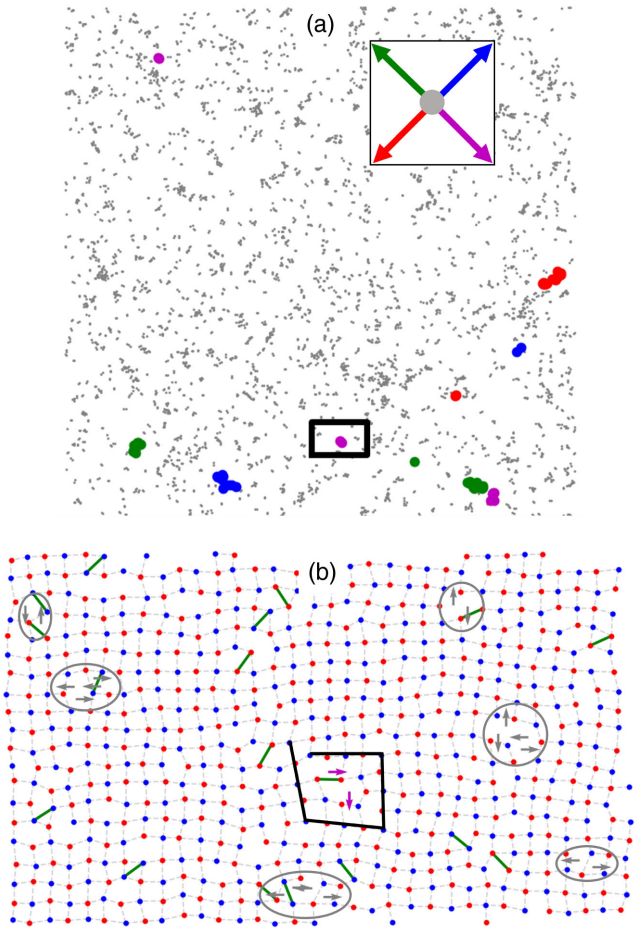

FIG. 3. Dislocations for a typical realization of $N = 90000$ spheres in the tetratic phase ($h = 0.8$ and $\rho_H = 0.81$). (a) The Burgers field, calculated using the DXA algorithm [36]. Dislocation-antidislocation pairs and larger neutral clusters are colored in gray. The remaining clusters, colored according to the direction of the total Burgers vector of the cluster, $\mathbf{b}_{\text{cluster}}$, all have magnitude $|\mathbf{b}_{\text{cluster}}| = \sqrt{2}$. (b) Enlargement of the black rectangle in (a). Here, individual spheres are shown in red or blue depending on their effective spin $s = \pm 1$. A free $\sqrt{2}$ dislocation cluster (magenta arrows) is surrounded by its Burgers circuit; the remaining dislocations (gray arrows) appear in neutral clusters (enclosed by gray ovals). Dashed gray lines show the bonds of the 4NN graph, used to quantify AF order; green lines are unsatisfied bonds.

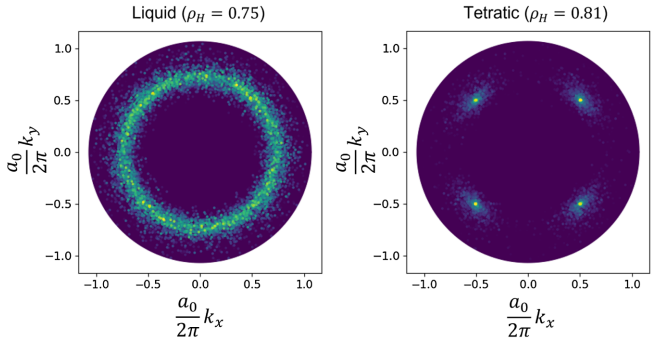

FIG. 4. Magnetic structure factor $S^M(\mathbf{k})$. Fairly sharp peaks, seen in the tetratic, are smeared into a ring in the liquid, indicating strong AF correlations in both phases.

in the liquid phase, we find a ring-shaped maximum in S^M of radius $\sqrt{2}\pi/a$, indicating that strong AF correlations survive even in the liquid.

We leave aside the question of the possible long-range nature of the AF order, and instead focus on quantifying the degree of antiferromagnetism in the system by comparing it to the ground state of the AF Ising model on a corresponding lattice. For this, we introduce a criterion for spheres to be considered neighbors, and define the four-nearest-neighbor (4NN) graph, as follows: Two spheres, α and β, are connected in the graph if and only if β is one of the four nearest neighbors of α and α is one of the four nearest neighbors of β. Figure 3(b) shows an example of the 4NN graph for a typical configuration in the tetratic phase. A number of bonds in this graph connect aligned effective spins, i.e., they are unsatisfied from the point of view of antiferromagnetism. The unsatisfied bonds in Fig. 3(b) are dilute and relatively isolated from one another. They occur due to large local fluctuations in sphere positions; near vacancies; or near a bound pair of single dislocations, which creates a short string of unsatisfied bonds connecting the pair. All of these effects can result in a local reorganization of the connectivity of the graph, and give rise to a small number of unsatisfied bonds that can be removed by performing *local* rearrangements of the spheres (or by adding individual spheres in the case of vacancies). By contrast, if the system had free single dislocations, this would lead to long strings of unsatisfied bonds joining faraway dislocations, and to large odd cycles that are not locally removable.

The degree of antiferromagnetism of a given hard-sphere configuration is captured by the fraction of unsatisfied bonds in the 4NN graph, f_{unsat}. We compare this to the degree of frustration of the graph f_{frust}, defined as the minimal value of f_{unsat} obtained when all possible spin configurations are considered. By definition, $f_{\text{frust}} \leq f_{\text{unsat}}$. Equivalently, f_{frust} is the fraction of unsatisfied bonds in the ground state of the AF Ising model, defined by the Hamiltonian [38] $H_{\text{Ising}} = \sum_{\langle\alpha,\beta\rangle} s_\alpha s_\beta$ where the sum runs over nearest neighbors in the 4NN graph. To find the ground state of H_{Ising}, we simulate the model at finite temperature T using the Metropolis algorithm [38], and slowly anneal from $T = 2.5$ to $T = 1/3$ starting from multiple random initializations of the Ising spins (the system effectively freezes below $T = 1/3$).

In Fig. 5, we see that f_{unsat} follows f_{frust} in the solid and tetratic phases. Hence, the effective spins in the hard-sphere system are as AF ordered as allowed by the lattice. This is a very strong result. In particular, the ability of the spins to be in the global minimum of f_{unsat}, despite the fact that the frustrated lattice is dynamical, is surprising. It suggests that

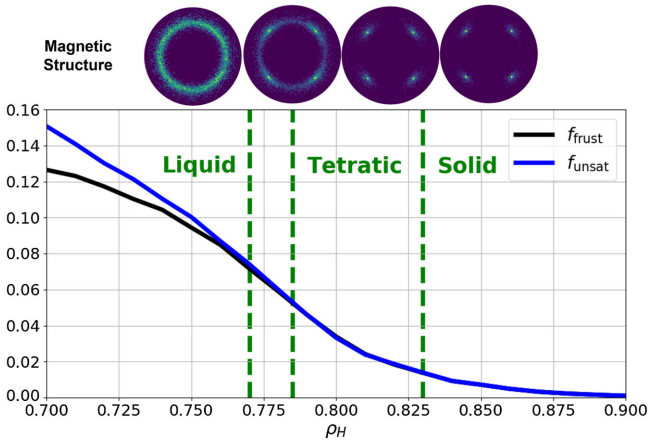

FIG. 5. Degree of frustration f_{frust} and fraction of unsatisfied bonds f_{unsat}, as function of sphere density. Note that the two closely match throughout the solid and tetratic phases. Top of the figure: evolution of the magnetic structure factor with ρ_H, for $\rho_H = 0.75$, 0.78, 0.81, and 0.85.

the lattice dynamics are strongly constrained by the spin configuration.

Before concluding, we note that the double dislocations can also be viewed as fundamental dislocations of the AF solid (with a two-site basis). However, this description can break down in the tetratic, where true long-range AF order is not established. In the tetratic, double dislocations are not compact objects. Rather, they appear as loose pairs of single dislocations, bound dynamically by the AF correlations. However, if the AF correlations were sufficiently short ranged then the string tension binding these dislocations would have vanished [39]. Then, the single dislocations would have become free objects.

In summary, we presented a novel phase, a topologically ordered tetratic, which separates solid and liquid phases in 2D systems with strong AF interactions. We demonstrated this phase numerically in a system of hard spheres confined between parallel plates, which may be realized experimentally using colloids. This phase has fairly sharp magnetic Bragg peaks and saturated AF correlations, despite being partially molten.

We thank Noga Bashan, Yariv Kafri, Dov Levine, Peter Lu, Yair Shokef, Avner Shultzman, Vincenzo Vitelli, and Uri Zondiner for useful discussions, and David Cohen for support in the use of the ATLAS cluster. We thank the Israel Science Foundation for financial support (Grant No. 1803/18).

[1] J. M. Kosterlitz and D. J. Thouless, J. Phys. C **6**, 1181 (1973).
[2] D. R. Nelson and B. I. Halperin, Phys. Rev. B **19**, 2457 (1979).
[3] A. P. Young, Phys. Rev. B **19**, 1855 (1979).
[4] L. Balents, M. P. A. Fisher, and C. Nayak, Phys. Rev. B **60**, 1654 (1999).
[5] S. Sachdev, Phys. Rev. B **45**, 389 (1992).
[6] L. Radzihovsky, Phys. Rev. A **84**, 023611 (2011).
[7] Z. Nussinov and J. Zaanen, J. Phys. IV **12**, 245 (2002).
[8] J. Zaanen and Z. Nussinov, Phys. Status Solidi (b) **236**, 332 (2003).
[9] J. A. Anderson, J. Antonaglia, J. A. Millan, M. Engel, and S. C. Glotzer, Phys. Rev. X **7**, 021001 (2017).
[10] T. Terao and Y. Oguri, Mol. Simul. **38**, 928 (2012).
[11] Z. Hou, Y. Zong, Z. Sun, F. Ye, T. G. Mason, and K. Zhao, Nat. Commun. **11**, 2064 (2020).
[12] K. W. Wojciechowski, D. Frenkel, and A. C. Brańka, Phys. Rev. Lett. **66**, 3168 (1991).
[13] K. Wojciechowski, Comput. Math. Sci. Technol. **10**, 235 (2004).
[14] E. N. Tsiok, Y. D. Fomin, E. A. Gaiduk, and V. N. Ryzhov, Phys. Rev. E **103**, 062612 (2021).
[15] A. Donev, J. Burton, F. H. Stillinger, and S. Torquato, Phys. Rev. B **73**, 054109 (2006).
[16] C. Avendaño and F. A. Escobedo, Soft Matter **8**, 4675 (2012).
[17] B. P. Prajwal and F. A. Escobedo, Novel mesophase behavior in two-dimensional binary solid solutions, arXiv:2004.02732.
[18] Y. D. Fomin, E. A. Gaiduk, E. N. Tsiok, and V. N. Ryzhov, Mol. Phys. **116**, 3258 (2018).
[19] B. Prajwal, J.-Y. Huang, M. Ramaswamy, A. D. Stroock, T. Hanrath, I. Cohen, and F. A. Escobedo, J. Colloid Interface Sci. **607**, 1478 (2022).
[20] T. Terao, J. Chem. Phys. **139**, 134501 (2013).
[21] I. V. Schweigert, V. A. Schweigert, and F. M. Peeters, Phys. Rev. Lett. **82**, 5293 (1999).
[22] I. Shamai and D. Podolsky, Molten antiferromagnets in two dimensions, arXiv:1801.08131.
[23] C. Timm, Phys. Rev. E **66**, 011703 (2002).
[24] J. L. Cardy, M. P. M. den Nijs, and M. Schick, Phys. Rev. B **27**, 4251 (1983).
[25] A. S. Meeussen, E. C. Oğuz, Y. Shokef, and M. v. Hecke, Nat. Phys. **16**, 307 (2020).
[26] C. Timm, S. M. Girvin, and H. A. Fertig, Phys. Rev. B **58**, 10634 (1998).
[27] M. Schmidt and H. Löwen, Phys. Rev. E **55**, 7228 (1997).
[28] Y. Shokef and T. C. Lubensky, Phys. Rev. Lett. **102**, 048303 (2009).
[29] Y. Han, Y. Shokef, A. M. Alsayed, P. Yunker, T. C. Lubensky, and A. G. Yodh, Nature (London) **456**, 898 (2008).
[30] E. P. Bernard, W. Krauth, and D. B. Wilson, Phys. Rev. E **80**, 056704 (2009).
[31] E. P. Bernard and W. Krauth, Phys. Rev. Lett. **107**, 155704 (2011).
[32] M. Engel, J. A. Anderson, S. C. Glotzer, M. Isobe, E. P. Bernard, and W. Krauth, Phys. Rev. E **87**, 042134 (2013).
[33] See Supplemental Material at http://link.aps.org/supplemental/10.1103/PhysRevLett.128.255501 for more details on the numeric simulations, and more observables which help to identify the phases.
[34] S. Ostlund and B. I. Halperin, Phys. Rev. B **23**, 335 (1981).

[35] W. Qi, A. P. Gantapara, and M. Dijkstra, Soft Matter **10**, 5449 (2014).

[36] A. Stukowski, Dislocation analysis tool for atomistic simulations, in *Handbook of Materials Modeling: Methods: Theory and Modeling*, edited by W. Andreoni and S. Yip (Springer International Publishing, Cham, 2020), pp. 1545–1558.

[37] A. Saxena, M. Prasad, A. Gupta, N. Bharill, O. P. Patel, A. Tiwari, M. J. Er, W. Ding, and C.-T. Lin, Neurocomputing **267**, 664 (2017).

[38] C. P. Robert and G. Casella, *Monte Carlo Statistical Methods*, Springer Texts in Statistics (Springer-Verlag, Berlin, Heidelberg, 2005).

[39] D. H. Lee and G. Grinstein, Phys. Rev. Lett. **55**, 541 (1985).